Picosecond radiography combined with other techniques to investigate microjetting from laser shock-loaded grooves

T. de Resseguier, C. Roland, G. Prudhomme, E. Brambrink, J.E. Franzkowiak, Didier Loison, E. Lescoute, A. Sollier, Laurent Berthe

HAL Id: hal-01874686
https://univ-rennes.hal.science/hal-01874686

Submitted on 12 Apr 2019

Picosecond Radiography Combined with Other Techniques to Investigate Microjetting from Laser Shock-loaded Grooves

T. de Rességuier[1, a)], C. Roland[1,2], G. Prudhomme[2], E. Brambrink[3,4], J.E. Franzkowiak[2], D. Loison[5], E. Lescoute[2], A. Sollier[2], L. Berthe[6]

[1] *Institut Pprime (UPR 3346), CNRS, ENSMA, Univ. Poitiers, F-86961 Futuroscope, France*
[2] *CEA, DAM, DIF, 91297 Arpajon, France*
[3] *LULI, CNRS, Ecole Polytechnique, CEA, Univ. Paris-Saclay, 91128 Palaiseau, France*
[4] *Sorbonne Universités, UPMC, Univ. Paris 06, CNRS, LULI, 75252 Paris, France*
[5] *Institut de Physique de Rennes, CNRS, Univ. Rennes 1, 35042 Rennes, France*
[6] *PIMM, CNRS, ENSAM-ParisTech, 151 Bd de l'Hôpital, 75013 Paris, France*

[a)] Corresponding author: resseguier@ensma.fr

Abstract. Debris ejection upon shock breakout at a rough surface is a key issue for many applications, including pyrotechnics and inertial confinement fusion. For a few years, we have used laser driven shocks to investigate microjetting in metallic samples with calibrated grooves in their free surface. Fast transverse optical shadowgraphy, time-resolved measurements of both planar surface and jet tip velocities, and post-shock analysis of recovered material have provided data over ranges of small spatial and temporal scales, short loading pulses (ns-order) and extremely high strain rates. The new experiment presented here involves two laser beams in a pump-probe configuration. Picosecond laser irradiation of a thin copper wire generates x-rays which are used to radiograph the microjets expanding from single grooves in tin and copper samples shock-loaded by a longer, nanosecond laser pulse. Such ultrashort radiography can be used to infer the density gradients along the jets as well as inside the samples deep beneath the grooves. Thus, combining this x-ray probe with the other experimental techniques mentioned above provides a more complete insight into the physics of microjetting at very high loading rates and the ballistic properties of the resulting ejecta.
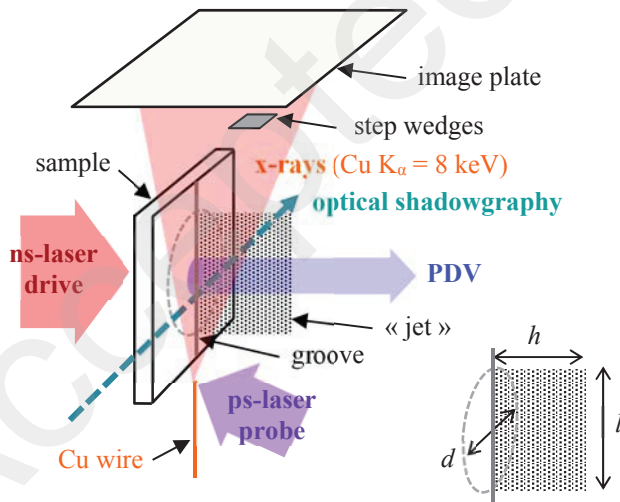
INTRODUCTION

Ejection of high velocity debris and their subsequent impacts are a safety issue for various applications involving shock waves, such as pyrotechnics or inertial confinement fusion. One of the processes governing debris generation from shock-loaded materials, sometimes referred to as microjetting, is the interaction of the shock front with a free surface presenting geometrical defects such as pits, scratches or grooves. It leads to the ejection of small (typically µm-scale) particles of high velocity (a few km/s) ahead of the main surface [e.g. 1-5]. In the past few years, we have studied this process under laser-driven shocks, over small spatial ($\sim$ µm) and temporal ($\sim$ ns) scales, at very high strain rates ($\sim 10^7$ s^{-1}), from straight grooves imprinted in the free surface of laser shock-loaded samples of various metals. To date, our main experimental results include (i) the determination of the mean velocities of both the planar free surface and the tips of the microjets expanding from the grooves, using fast optical shadowgraphy [6-8] ; (ii) time-resolved measurements of these velocities using Photonic Doppler Velocimetry (PDV, also known as Heterodyne Velocimetry) [6, 9] ; (iii) some post-shot evidence of the jetting process and the effect of spall fracture, from microscopic examination of recovered samples [6, 8] ; (iv) direct observation of the late stage of jet fragmentation into distinct debris, using transverse optical shadowgraphy [9] ; and (v) an attempt to characterize ejecta size distributions using soft recovery in a gel and x-ray tomography [10]. Yet, the mass distribution in the jets, which is a key issue for the practical applications mentioned above, is still largely unknown in our experiments.

Besides, some of our post-recovery observations and velocity data have raised questions on wave interactions occurring inside the bulk material and edge effects at the grooves sides [7].

Here, we report the implementation of a new, laser based, ultrafast radiography technique which was recently added to our experimental instrumentation to investigate the mass density along a jet expanding from a single groove of triangular shape, as well as tension inside the bulk sample beneath the groove edges. The application of this same technique to characterize material ejection from periodic grooves of approximately sinusoidal shapes and different shape factors in laser shock-melted tin is described in another contribution [11].
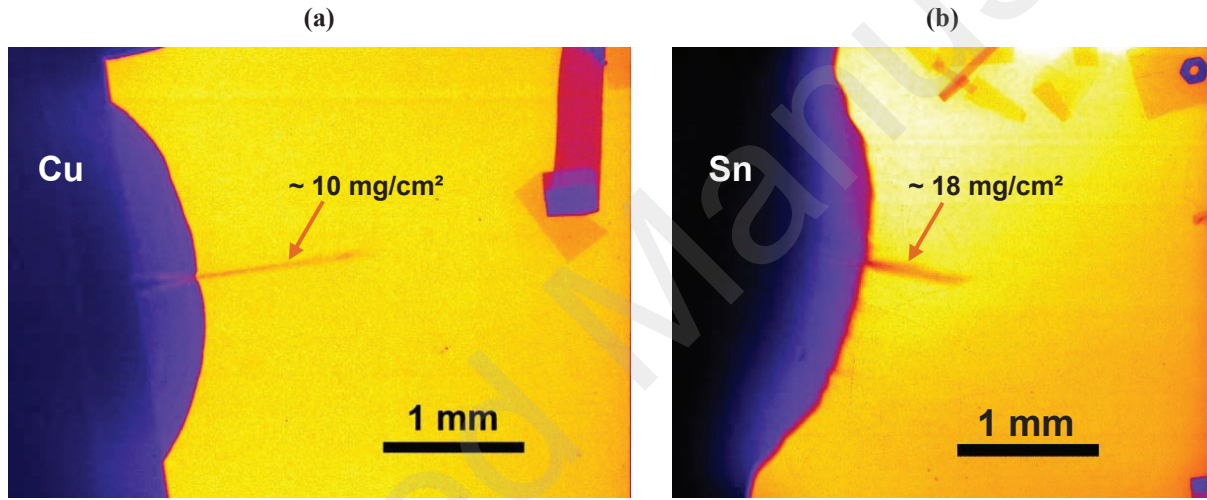
EXPERIMENTAL TECHNIQUE

The experiments were performed in the *nano2000* facility of the *Laboratoire pour l'Utilisation des Lasers Intenses* (LULI, France). Shock loading was driven by a ~ kJ-energy, 5 ns-duration, 1.06 μm-wavelength laser pulse focused on a spot of diameter *d* (a few mm) in the sample surface, in vacuum to avoid laser breakdown in air. Opposite to this loaded spot, the grooved free surface was monitored with a collimated PDV probe recording both planar surface velocity and jet tip velocity. A second laser pulse of ~10 J-energy and 1.5 ps-duration is focused onto the tip of a freestanding, vertical Cu wire of 20 μm-diameter set a few mm below the sample free surface (Fig. 1). This intense (~2 ×10^{18} W/cm^2) irradiation creates energetic electrons and generates x-rays through the emission of K-shell radiation, at 8 keV for Cu. Some of these x-rays are transmitted through the sample and the jets to an horizontal Image Plate (IP), which provides in-situ radiography of the ejecta behind the shock-loaded sample at a given instant after shock breakout, accurately controlled by adjusting the time delay between the ns-drive and the ps-probe (400 ns in the shots reported here). The duration of the x-ray burst is only slightly longer than the ps laser pulse [12] so that temporal resolution is very good. The use of a thin wire as a backlighter target minimizes the source size to ensure a good spatial resolution too. The IP is set a few tens of cm above the sample, so the radiographs are recorded with a magnification of about 21×. The geometry depicted in Fig. 1, with normal irradiation of the wire by the ps-laser and the IP placed normal to the wire, was demonstrated to be the most relevant for resolution, homogeneity and contrast of the x-ray signal [12]. After each shot, the IP was scanned to measure the photo-stimulated luminescence (PSL), proportional to the x-ray yield. To correlate this PSL value to mass density, step wedges of Cu and Sn with thicknesses ranging from 5 μm to 100 μm were inserted in front of the IP. This on-shot calibration removes uncertainties due to shot-to-shot fluctuations [12, 13]. It is illustrated in more details in the next section. Finally, the spatial resolution was found to be about 20 μm by performing a static radiography of a 300 lpi-grid located at the sample position (details can be found elsewhere [11]).

FIGURE 1. Schematic of the experimental setup. The irradiation of a freestanding Cu wire by a ps-duration laser pulse generates an x-ray burst which is used to radiograph the jet expanding from a groove in the free surface of a sample subjected to a ns-laser driven shock. PDV measurement and optical shadowgraphy are performed simultaneously along other directions. In this configuration referred to as "sideways" in this paper, radiography is performed along the groove direction.

"SIDEWAYS" RADIOGRAPHY

Fig. 2 shows digitized images of two typical radiographs recorded behind Cu (a) and Sn (b) samples, in the configuration shown in Fig. 1, referred to as "sideways" radiography, along the groove direction. Step wedges of Cu and Sn with different thicknesses are visible at the top right of both images. Such step wedges direct correlation between transmitted x-ray intensity (color scale) and areal mass density. Data analysis is illustrated in Fig. 3, corresponding to the shot in Fig. 2b. It shows the raw radiograph (Fig. 3a), where PSL levels are measured in rectangular zones of interest (blue frames around the jet and the step wedges) and divided by the mean background level measured in their close vicinity (green frames), respectively. This somewhat accounts for the non-uniform background level over the IP, like in Fig. 2b. Then, a correlation between PSL and thickness is inferred from the step wedges, using a Beer-Lambert fit (Fig. 3b). Finally, this fit is used to convert PSL into areal mass density in and near the jet (Fig. 3c). Thus, the resulting estimates of the areal mass m_a along the jets are about 10 mg/cm² and 18 mg/cm² in Fig. 2a and 2b, respectively. Assuming a uniform particle distribution in the transverse direction, over the width l of the jet supposed to be roughly equal to the diameter d of the loaded spot (see the sketch at the bottom right in Fig. 1), the average mass density in the jet can be evaluated as $\rho_j = m_a / d$, about ~ 36 mg/cm³ in Fig. 2a (Cu) and ~ 60 mg/cm³ in Fig. 2b (Sn).

(a)   **(b)**
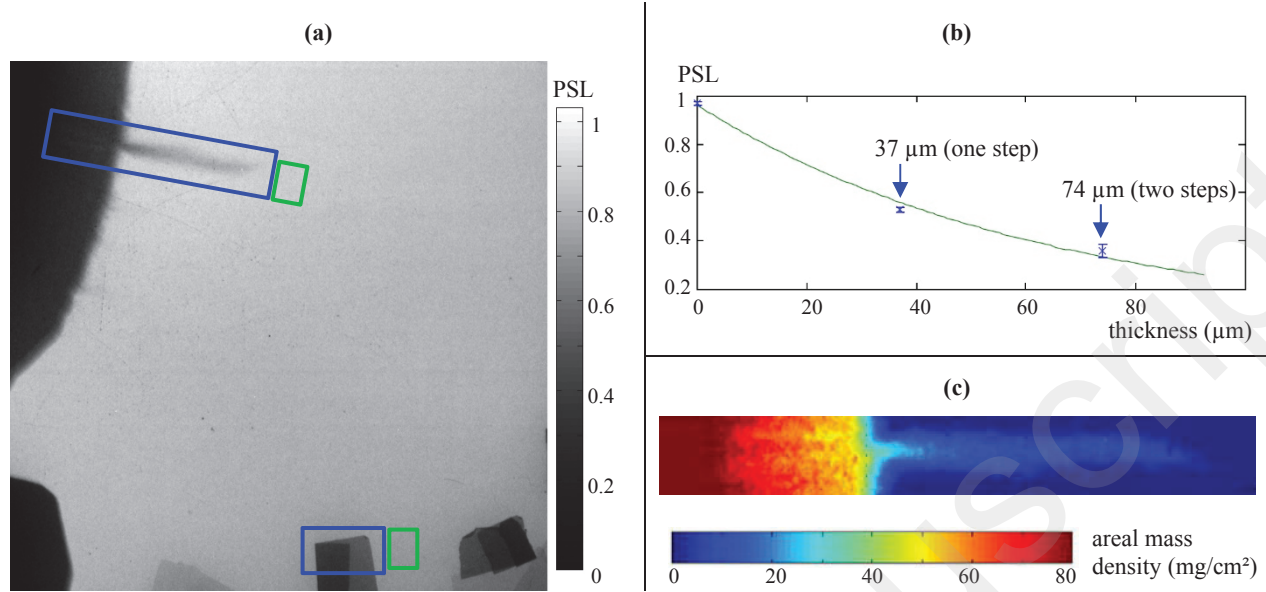

FIGURE 2. Typical radiographs recorded behind Cu and Sn samples subjected to laser shock loading (onto their left surface, not shown), showing jetting from a straight groove in their free surface. **(a)** : Cu sample, 250 µm-thick, groove of 20° half-angle, loaded spot of 2.8 mm-diameter, shock breakout pressure 34 GPa ; **(b)** : Sn sample, 260 µm-thick, groove of 30° half-angle, loaded spot of 3.0 mm-diameter, shock breakout pressure 20 GPa. The time delay between the ns-drive (laser shock) and the ps-probe (x-ray burst) is 400 ns in both shots.

The radiographs also show very clearly (although more clearly in Cu than in Sn) two lines of low density (pink color in both images) deep inside the bulk sample, between the loaded side (left side) and both edges of the groove. They probably result from local tension due to the interactions of the incident unloading wave with the rarefaction waves reflected from the groove edges [6]. Numerical simulations are under way to understand these effects in more details [9, 10].

Finally, like stated above and depicted in Fig. 1, fast optical shadowgraphy is performed simultaneously along the horizontal direction. As detailed elsewhere [6, 7], it provides mean velocities of the free surface (1.49 km/s in the shot on Cu, 1.51 km/s in that on Sn), and of the jet tip (4.6 km/s in the shot on Cu, 4.0 km/s in that on Sn), consistent with the radiographs and with velocity data obtained previously [6, 9].
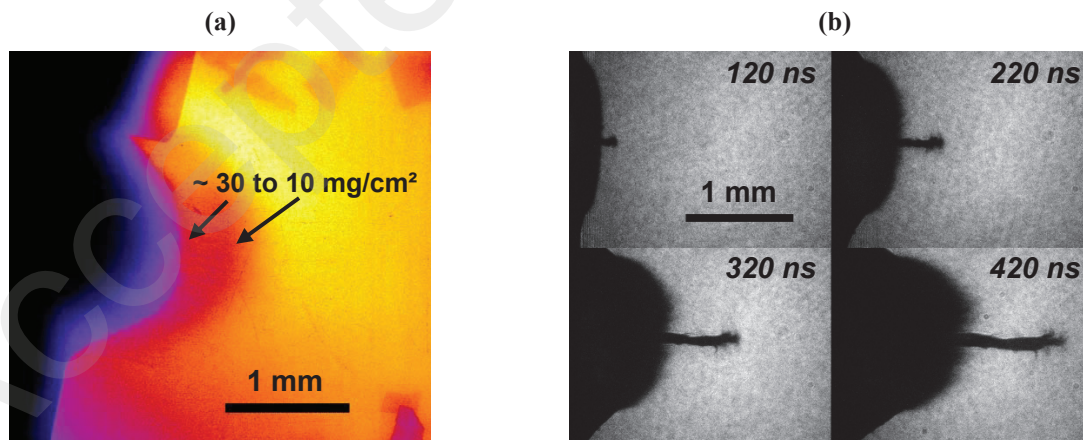
FIGURE 3. Illustration of radiography analysis for the record shown in Fig. 2b : raw radiograph (a), PSL-thickness correlation (b), and areal mass density in and near the jet (c).

"IN-PLANE" RADIOGRAPHY

Fig. 4a shows another example of radiograph of a Sn sample where the groove direction is normal to the wire, unlike in Fig. 1. In this "in-plane" configuration, the mass density can be evaluated without integrating along the jet width, while the optical shadowgraphs show jetting "from the side" (Fig. 4b). Based on the transmission through the step wedges, a gradient of areal mass density along the expanding jet can be roughly inferred, from about 30 at the bottom to 10 mg/cm² at the tip. In this high intensity shot, focused on a 1.5 mm-diameter spot, measured velocities of the planar free surface and of the jet tip are 2.9 km/s and 5.7 km/s, respectively. Shock breakout pressure is 50 GPa, well above the pressure range over which Sn is expected to melt on release [14, 15]. Thus, the free surface is actually the contour of an expanding cloud of tiny droplets (so-called microspall [16]), with a more blurry aspect than in Fig. 2b where Sn remained solid beneath the free surface.

FIGURE 4. Microjetting behind a 260 µm-thick Sn sample with a groove of 30° half-angle under a laser shock applied on a 1.5 mm-diameter spot, leading to a shock breakout pressure of 50 GPa. **(a)** : radiograph recorded 400 ns after the ns-laser shot, in the "in-plane" radiography configuration (i.e. normal to the groove direction) ; **(b)** : shadowgraphs recorded simultaneously in the other direction (i.e. along the groove direction) with 5 ns-exposure times, at successive instants after the ns-laser shot.

From the shadowgraphs in Fig. 4b, jet thickness is evaluated to about 70 μm. Hence, like in the previous section, the mean density in the jet ρ_j can be estimated as 1.4 g/cm^3 (using the ~ 10 mg/cm^2 areal mass measured near the jet tip). This is about 20 times higher than in the lower pressure shot in Fig. 2b. Such increase is consistent with the effect of melting which was shown to sharply enhance the amount of shock-produced ejecta [3].

CONCLUSION

A short-pulse laser-generated K$_\alpha$ x-ray source was used to radiograph the jets expanding from single grooves of triangular shape in the free surface of laser shock-loaded Cu and Sn samples. High quality radiographs with good spatial and temporal resolution were obtained. Step wedges were introduced at each shot to correlate x-ray transmission with areal mass densities. Further work is under way to improve this calibration. Nevertheless, direct estimations of the ejecta mass distributions along the jets could be provided, as well as some new insight into the tension induced deep inside the bulk samples, below the jets, from both sides of the grooves. Thus, this ultrafast radiography technique, fully compatible with PDV measurements and optical shadowgraphy, performed simultaneously in other directions (see Fig. 1), offers a means for a complete characterization of the ballistic properties (i.e. mass and velocity distributions) of the ejecta, to be understood and anticipated to efficiently protect nearby equipment against their impacts.

ACKNOWLEDGMENTS

REFERENCES

1. J. R. Asay, L. P. Mix and F. Perry, Appl. Phys. Letters **29**, 284 (1976).
2. P. Andriot, P. Chapron and R. Olive, AIP Conf. Proc. **78**, pp. 505-508 (1981).
3. M. B. Zellner, W. V. McNeil, J.E. Hammerberg, R.S. Hixson, A.W. Obst, R.T. Olson, J. R. Payton, P.A. Rigg, N. Routley, G. D. Stevens, W. D. Turley, L. Veeser and W. T. Buttler, J. Appl. Phys. **103**, 123502 (2008).
4. A. L. Mikhailov et al., J. Exp. And Theor. Phys. **118**, pp. 785-797 (2014).
5. D. S. Sorenson, R. W. Minich, J. L. Romero, T. W. Tunnell and R. M. Malone, J. Appl. Phys. **92**, 5830 (2002).
6. T. de Rességuier, E. Lescoute, A. Sollier, G. Prudhomme and P. Mercier, J. Appl. Phys. **115,** 043525 (2014).
7. T. de Rességuier, C. Roland, G. Prudhomme, E. Lescoute, D. Loison, P. Mercier, J. Appl. Phys. **119** (18), 185108 (2016).
8. T. de Rességuier, C. Roland, E. Lescoute, A. Sollier, D. Loison, L. Berthe, G. Prudhomme, P. Mercier, AIP Conf. Proc. 1793, 100025 (2017).
9. C. Roland, T. de Rességuier, A. Sollier, E. Lescoute, D. Loison, L. Soulard, J. of the Dynamic Behavior of Materials **3** (2), 156-163 (2016).
10. C. Roland et al., *submitted to this conference*.
11. G. Prudhomme et al., *submitted to this conference*.
12. E. Brambrink, H.G. Wei, B. Brabrel, P. Audebert, A. Benuzzi, T. Boehly, T. Endo, C. Gregory, T. Kimura, R. Kodama, N. Ozaki, M. Rabec le Gloahec, M. Koenig, Phys. of Plasmas **16**, 033101 (2009).
13. E. Brambrink, H.G. Wei ; B. Barbrel, P. Audebert, A. Benuzzi-Mounaix, T. Boehly, T. Endo, C. Gregory, T. Kimura, R. Kodama, N. Ozaki, H.S. Park, M. Koenig, Phys. Rev. E **80**, 056407 (2009).
14. C. Mabire, P.L. Hereil, AIP Conf. Proc. **505**, pp. 93-96 (2000).
15. W.T. Buttler, D.M. Oro, D.L. Preston, K.O. Mikaelian, F.J. Cherne, R.S. Hixson, F.G. Mariam, C. Morris, J.B. Stone, G. Terrones, D. Tupa, J. Fluid Mech. **703**, pp. 60-84 (2012).
16. D. Loison, T. de Rességuier, A. Dragon, P. Mercier, J. Bénier, G. Deloison, E. Lescoute, A. Sollier, J. Appl. Phys. **112**, 113520 (2012).